IEEE Photonics Journal
An IEEE Photonics Society Publication

$(In_xGa_{1-x})_2O_3$ Photodetectors Fabricated on Sapphire at Different Temperatures by PLD

Volume 10, Number 3, June 2018

Ke Zhang
Qian Feng
Lu Huang
Zhuangzhuang Hu
Zhaoqing Feng
Ang Li
Hong Zhou
Xiaoli Lu
Chunfu Zhang
Jincheng Zhang
Yue Hao

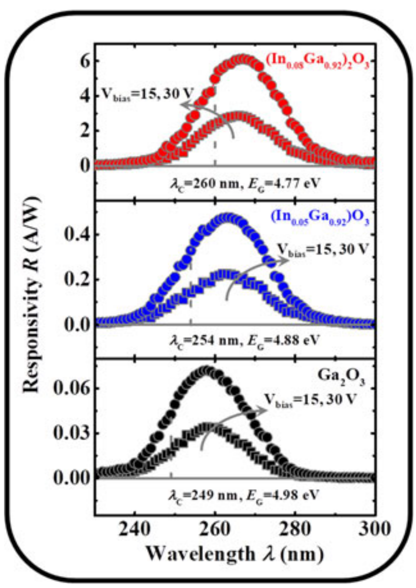

DOI: 10.1109/JPHOT.2018.2841968

$(In_xGa_{1-x})_2O_3$ Photodetectors Fabricated on Sapphire at Different Temperatures by PLD

Ke Zhang, Qian Feng, Lu Huang, Zhuangzhuang Hu, Zhaoqing Feng, Ang Li, Hong Zhou, Xiaoli Lu, Chunfu Zhang, Jincheng Zhang, and Yue Hao

Wide Bandgap Semiconductor Technology Disciplines State Key Laboratory, Xidian University, Xi'an 710071, China

DOI:10.1109/JPHOT.2018.2841968

Manuscript received April 4, 2018; revised May 24, 2018; accepted May 26, 2018. Date of publication May 29, 2018; date of current version June 18, 2018. This work was supported by the National Natural Science Foundation of China (NSFC) under Grant Nos. 61334002, 61774114 and the National 111 Center (Grant No. B12026). Corresponding authors: Qian Feng and Jincheng Zhang (e-mail: qfeng@mail.xidian.edu.cn; jchzhang@xidian.edu.cn).

Abstract: The $(In_xGa_{1-x})_2O_3$ photodetectors were fabricated on the single-crystalline $(In_xGa_{1-x})_2O_3$ films deposited on sapphire substrate by pulsed laser deposition. The structural and optical properties of the epilayers were investigated using high-resolution X-ray diffraction, X-ray photoelectron spectroscopy, spectroscopic ellipsometry, and transmittance spectra. With decreasing the growth temperature, the indium composition increased and the bandgap decreased from 4.99 eV to 4.89 eV $(In_{0.05}Ga_{0.95})_2O_3$ and 4.78 eV $(In_{0.08}Ga_{0.92})_2O_3$. Furthermore, the photoelectrical characteristics of $(In_xGa_{1-x})_2O_3$ detectors were also studied. The enhanced I_{photo}, I_{dark}, and responsivity R were achieved in the devices with higher In composition, while a larger number of defects were introduced, resulting in the significant persistent photoconductivity.

Index Terms: $(In_xGa_{1-x})_2O_3$, photodetectors, temperatures, PLD.

1. Introduction

Recently, Ga_2O_3 has attracted great attention for high power electronic and ultraviolet (UV) or deep-ultraviolet (DUV) applications because of its exceptional properties, such as large bandgap (E_G), high theoretical breakdown electric field and physical and chemical stabilities, etc. [1]–[5]. There exists five polymorphs of Ga_2O_3 (α, β, γ, δ and ε phases), among which β-Ga_2O_3 is the most common and most stable crystal. β-Ga_2O_3 photodetectors have been fabricated and characterized with the cutoff wavelength around 250 nm [6]–[8]. It is known that the E_G can be tuned by incorporating Al or In into β-Ga_2O_3 to broaden the photodetection range. $(In_xGa_{1-x})_2O_3$ films have been deposited by various methods: metal organic chemical vapor deposition (MOCVD) [9], molecular beam epitaxy (MBE) [10], Sol-gel [11], and pulsed laser deposition (PLD) [12]. So far, a few studies have been carried out on the growth of $(In_xGa_{1-x})_2O_3$ epilayers and the fabrication of $(In_xGa_{1-x})_2O_3$ photodetectors [11], [13].

In this paper, the single-crystalline $(In_xGa_{1-x})_2O_3$ films were deposited on c-plane sapphire substrates by PLD. The properties of the $(In_xGa_{1-x})_2O_3$ epilayers were investigated by High resolution X-ray diffraction (HRXRD), X-ray photoelectron spectroscopy (XPS), spectroscopic ellipsometry

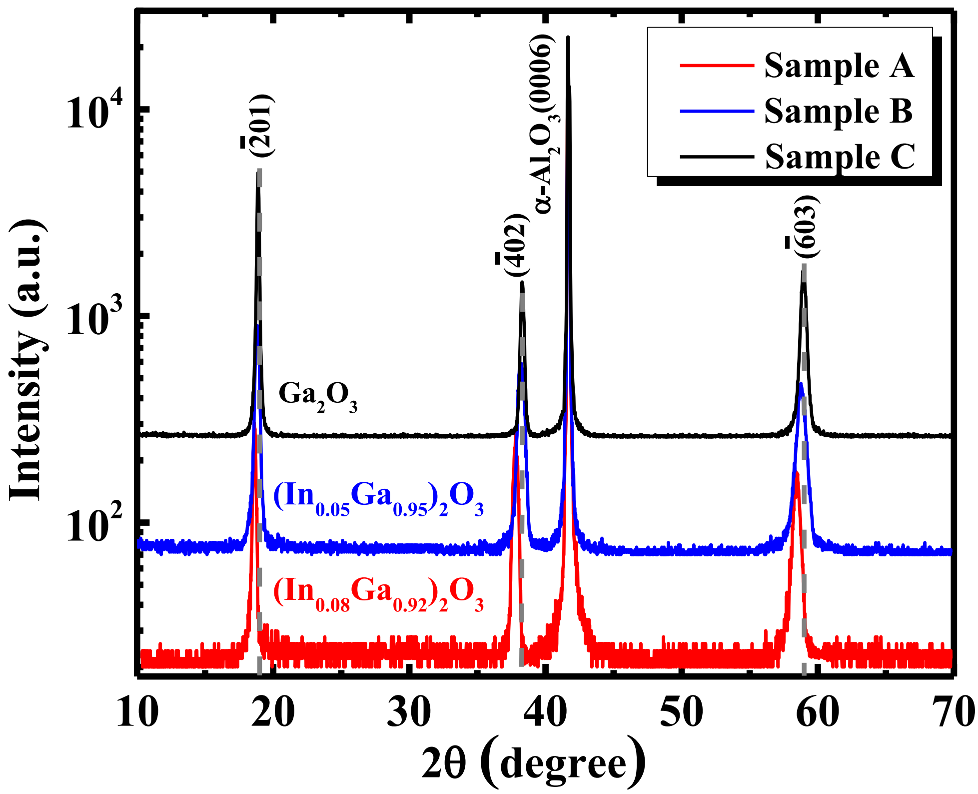

Fig. 1. HRXRD diffraction curves of $(In_xGa_{1-x})_2O_3$ and Ga_2O_3 samples on sapphire. The peaks of $(In_xGa_{1-x})_2O_3$ are located at the left side of Ga_2O_3 peaks.

(SE) and transmittance spectra. The $(In_xGa_{1-x})_2O_3$ photodetectors were fabricated and characterized with different In composition. Compared with Ga_2O_3 photodetectors, the cutoff wavelength of $(In_xGa_{1-x})_2O_3$ devices could be tuned from 253 nm($x = 0$) to 335 nm ($x = 1$), which may be widely used in military and civil applications, such as flame detection, early missile threat warning. In our work, the better performance has been achieved in $(In_xGa_{1-x})_2O_3$ photodetectors, including photocurrent and responsivity, although the cutoff wavelength only changes from 249 nm(Ga_2O_3 on sapphire substrate) to 254 nm ($x = 0.05$) and 260 nm($x = 0.08$).

2. Experiments

$(In_xGa_{1-x})_2O_3$ films were grown on double-polished (0001)-oriented sapphire substrates using PLD method. The ceramic $(In_xGa_{1-x})_2O_3$ with In composition of $x = 0.10$ was used as target. The KrF excimer laser with a frequency of 3 Hz and the energy density of 2.0 J/cm^2 was applied to irradiate the target. The $(In_xGa_{1-x})_2O_3$ epilayers were deposited in a lower oxygen pressure of 0.003 mbar at the temperatures of 500 °C(sample A) and 550 °C(sample B), respectively. The Ga_2O_3 epilayer was also grown as a reference (Sample C). For the photodetectors fabrication, the interdigital Ti/Au (10 nm/100 nm) films were deposited using electron beam evaporation as the schottky contacts, with the finger spacing of 100 μm and the total length of 17.5 mm.

3. Results and Discussion

3.1 Material Characterization

The structural properties of the samples were investigated by HRXRD using CuKα radiation at room temperature. Fig. 1 shows the HRXRD curves of the three samples. There are four diffrac-

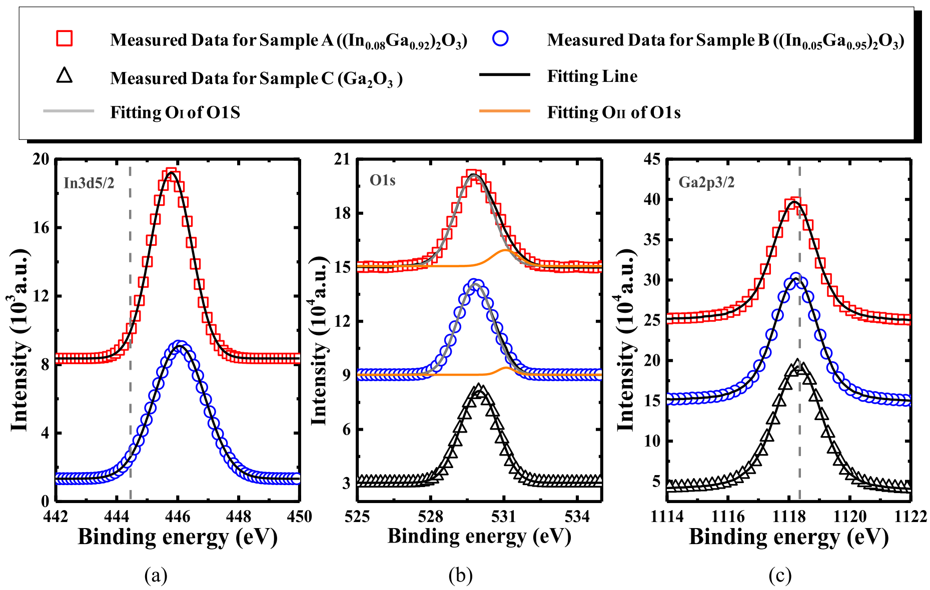

Fig. 2. XPS spectra of (a) In3d5/2, (b) O1s and (c) Ga2p3/2 for $(In_xGa_{1-x})_2O_3$ and Ga_2O_3 samples.

tion peaks corresponding to the $(\bar{2}01)$, $(\bar{4}02)$ and $(\bar{6}03)$ planes of β-$(In_xGa_{1-x})_2O_3$ and sapphire substrate (0006) planes, respectively. The $(In_xGa_{1-x})_2O_3$ peaks are located at the lower angle side in comparison with the Ga_2O_3 peaks, demonstrating that In atoms have been incorporated into the lattice of β-$Ga_2O_3$0. In addition, the peaks of $(In_xGa_{1-x})_2O_3$ shift to lower angle as the temperature decreasing to 500 °C, indicating more In atoms in sample A than sample B. According to Bragg's equation, the interplanar spacings *d* of $(\bar{2}01)$, $(\bar{4}02)$ and $(\bar{6}03)$ planes for the three samples are 0.4726, 0.2368 and 0.1578 nm (sample A), 0.4706, 0.2354 and 0.1570 nm (sample B), 0.4594, 0.2348 and 0.1566 nm (sample C), in good agreement with $(In_xGa_{1-x})_2O_3$ films deposited by continuous composition spread (CCS) PLD [15].

Fig. 2 presents the XPS peaks of In3d5/2, O1s and Ga2p3/2 for $(In_xGa_{1-x})_2O_3$ samples. Before XPS measurement, the surface of the samples was etched by *in situ* Ar^+ ion and the binding energy was calibrated using the C1s line (284.6 eV) from adventitious carbon. With In composition increment, In3d5/2 peak shifts toward In3d5/2 of In_2O_3 (444.5 eV) and Ga2p3/2 peak deviates from Ga2p3/2 of Ga_2O_3 (1118.3 eV), as shown in Fig. 2(a) and (c), indicating that Ga atoms have been effectively substituted by In atoms [16]. Based on the area of the peaks and the corresponding sensitivity factors, In composition of $(In_xGa_{1-x})_2O_3$ films are calculated to be 8% and 5% for the sample A and B. Fig. 2(b) shows the Gaussian fitting results of O1s peaks. The oxygen vacancies can be determined by calculating the area ratio $(O_{II}/O_I + O_{II})$, where O_I and O_{II} are associated with O^{2-} ions surrounded by Ga/In atoms and oxygen vacancies in the epilayers [13], [17]. The ratios are about 13% and 6% for sample A and B, indicating more oxygen vacancies introduced in the sample A.

The variable-angle spectral ellipsometry was used to determine the thicknesses, refractive index *n* (Fig. 4(a)) and extinction coefficient *k* (Fig. 4(b)) at room temperature. The incidence angles were set to 55°, 65° and 75° in the 200–800 nm spectral range. The Cauchy dispersion fitting and point-by-point method were applied for 400–800 nm and 200–400 nm spectra range, respectively [18], [19]. Fig. 3 presents the fitting results with the thickness of 358, 320 and 198 nm for the three samples. The refractive index *n* increases with the In composition, which is similar to the reference [19]. The extinction coefficient *k* of $(In_xGa_{1-x})_2O_3$ expilayers is higher than that of Ga_2O_3 control and the absorption edge shifts toward longer wavelength as Fig. 4(b) shown, indicating that $(In_xGa_{1-x})_2O_3$ films have narrower bandgap depending on the In composition x. For the higher extinction coefficient *k* of $(In_xGa_{1-x})_2O_3$ sample, the thickness can be reduced in comparison with

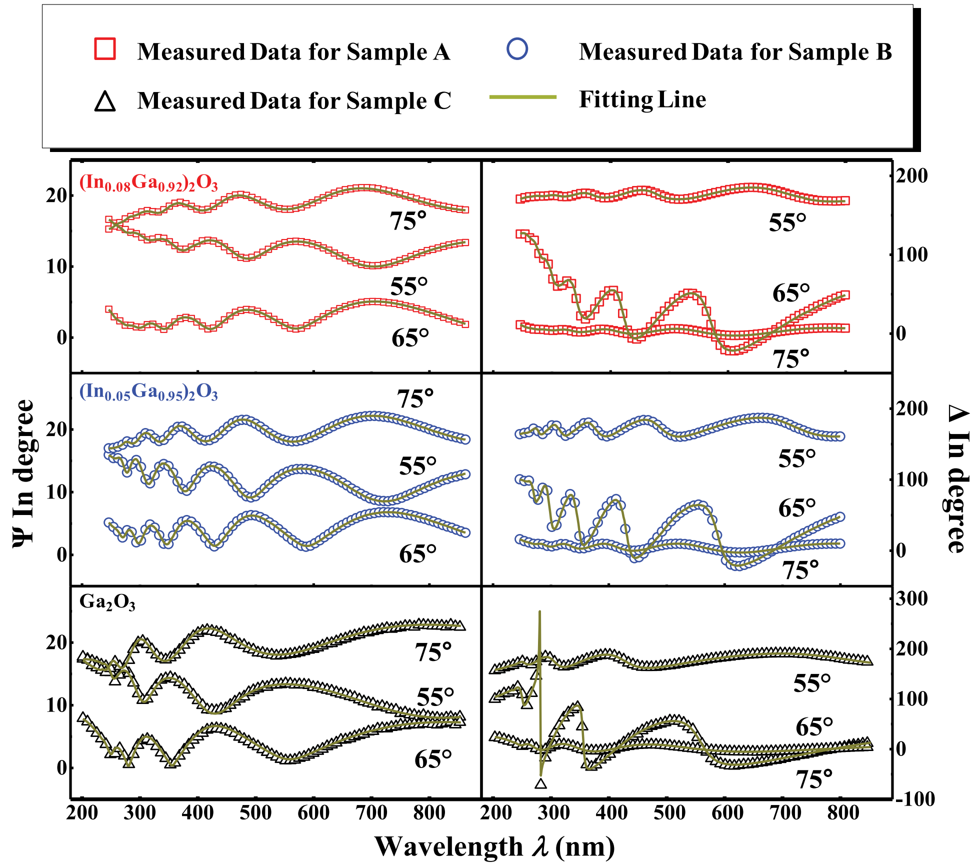

Fig. 3. SE measured data of Ψ (left) and Δ (right) and the fitting line of (In$_x$Ga$_{1-x}$)$_2$O$_3$ and Ga$_2$O$_3$ samples at angles of 55°, 65° and 75°.

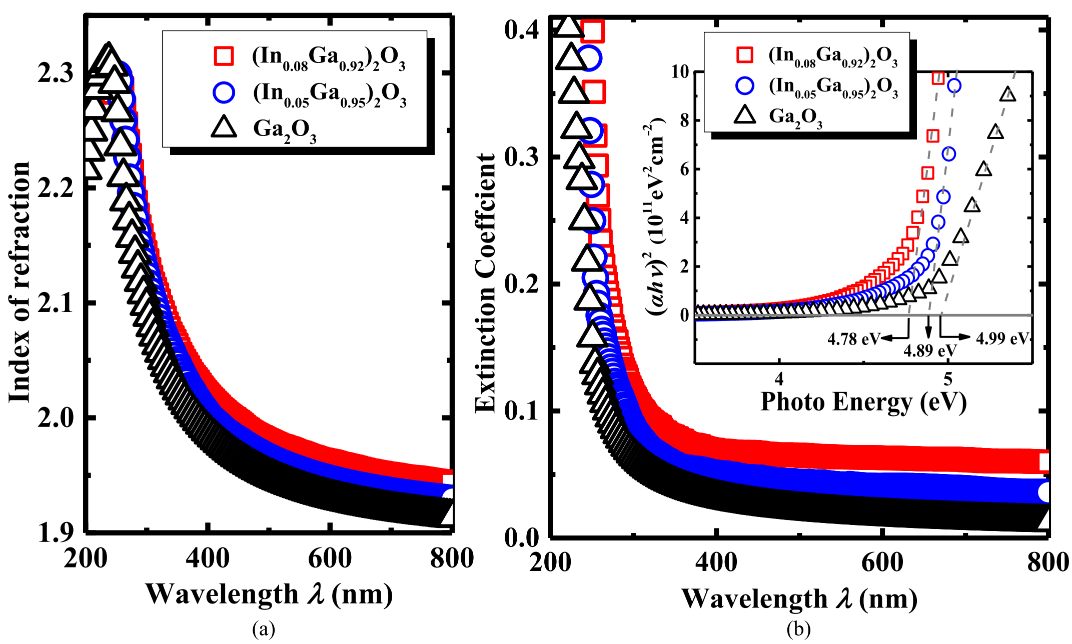

Fig. 4. Spectra of (a) the refractive index (n) and (b) the extinction coefficient (k) for the three samples and the inset is E_G for different samples calculated by the extinction coefficient.

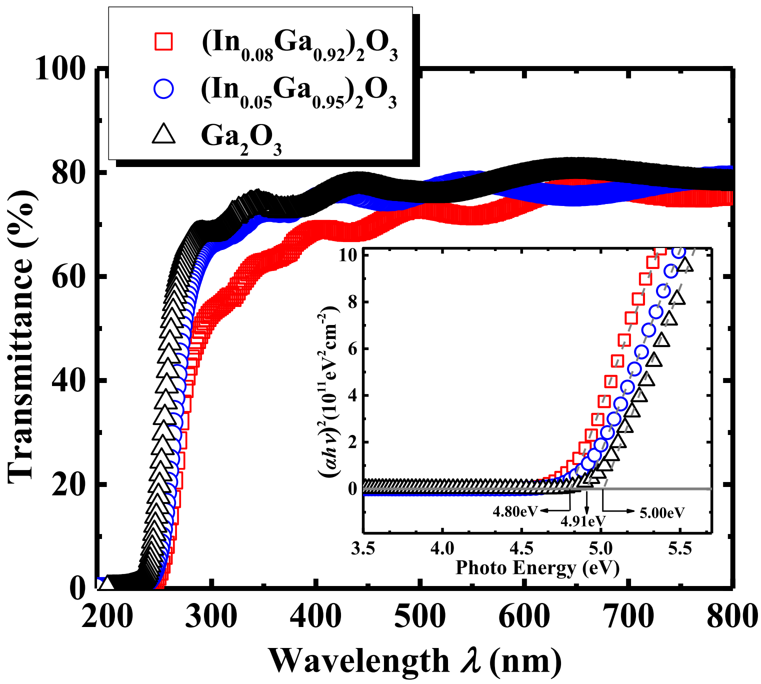

Fig. 5. Transmittance spectra of $(In_xGa_{1-x})_2O_3$ and Ga_2O_3 films and the inset is $(\alpha h\nu)^2$ as the function of $h\nu$ for the three samples.

Ga_2O_3 film to adequately absorb the incident light. The Ga_2O_3 and $(In_xGa_{1-x})_2O_3$ photodetectors can be both widely used in the civil and military applications, such as missile tracking, fire detection, ozone holes monitoring, chemical/biological analysis. The E_G of $(In_xGa_{1-x})_2O_3$ films can be obtained by extrapolating the linear region of $(\alpha h\nu)^2$ $h\nu$ to the horizontal axis, where $h\nu$ is the energy of the incident photon and α is the absorption coefficient of the films, which can be calculated by the relation $\alpha = 4\pi k/\lambda$. Therefore, the bandgap E_G can be found to be 4.78, 4.89 and 4.99 eV, respectively, as depicted in the inset of Fig. 4(b).

The optical transmittance spectra of the samples are shown in Fig. 5. The average transmittance is beyond 70% in the visible region and a sharp absorption edge can be observed. With increasing In content, the absorption edge shifts toward longer wavelength. In addition, the absorption coefficient α can also be calculated by the relation $\alpha = (1/t)\ln[(1 - R_c)^2/T]$ [20], where t is the thickness and R_c and T are the reflectance and transmittance, respectively. The thicknesses of the epilayers were determined by SE discussed above. For the transmittance greater than 70% with the λ longer than 400 nm, the reflectance about 30% was adopted to determine α. Then E_G of the three samples are 4.80, 4.91, and 5.00 eV, respectively, in good agreement with the SE results.

3.2 Photoelectric Characteristics of the Devices

The photoelectrical characteristics of $(In_xGa_{1-x})_2O_3$ photodetectors were investigated using a UV lamp, including the dark current I_{dark}, photocurrent I_{photo}, time-dependent photoresponse and the responsivity R. Fig. 6(a)–(c) represents the I_{photo} versus the bias voltage V_{bias} with a normalized optical power density P_{light} of 0, 300, 600 and 900 $\mu W/cm^2$ and (d) is the dark current I_{dark} plotted on a logarithmic scale. The I_{dark} and I_{photo} of $(In_xGa_{1-x})_2O_3$ devices are higher than that of Ga_2O_3. The larger I_{dark} may be related to the enhancement of $(In_xGa_{1-x})_2O_3$ conductivity [21]. During illumination, a large number of electron-hole pairs would be generated and the holes drift to cathode electrode, resulting in the decrease of Schottky barrier height at the ground contact, more electrons injection into the channel. In addition, the effective Schottky barrier height of $(In_xGa_{1-x})_2O_3$ devices

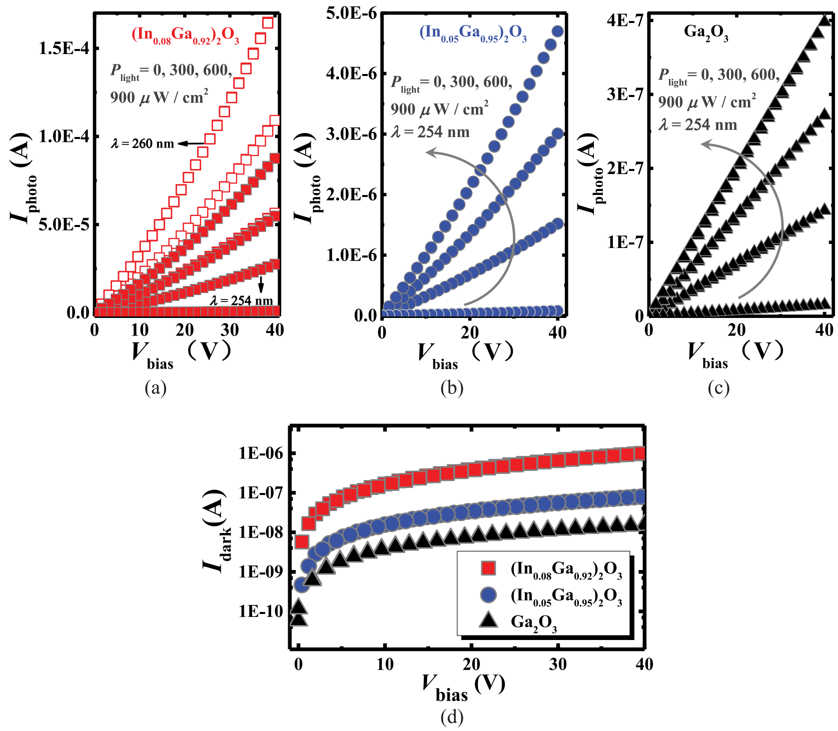

Fig. 6. The linear photocurrent for (a) $(In_{0.08}Ga_{0.92})_2O_3$, (b) $(In_{0.05}Ga_{0.95})_2O_3$ and (c) Ga_2O_3 devices under 254 or 260 nm illumination with various P_{light} and (d) The logarithmic dark current I_{dark} versus V_{bias} for the three samples.

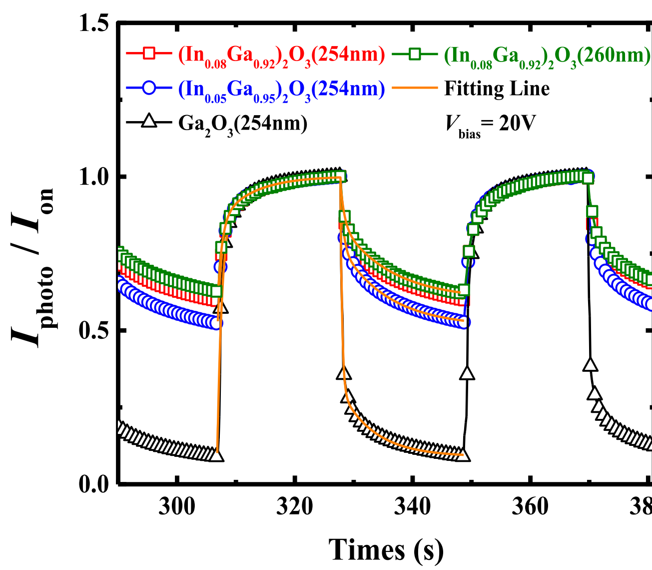

Fig. 7. Time-dependent I_{photo} characteristics and the fitting line of the rise and decay process for different photodectors at $V_{bias} = 20$ V and $\lambda = 254$ or 260 nm.

will also be reduced with In composition [22], [23]. As a result, more extra carriers can be collected, leading to the boosting I_{photo}.

Fig. 7 depicts the typical time-dependent photoresponse characteristics of fabricated photodetectors. During the measurements, an illumination λ of 254 nm (or 260 nm) square-wave light was used with V_{bias} of 10 V, P_{light} of 300 μW/ cm^2 and period of 40 s. The rise and decay processes

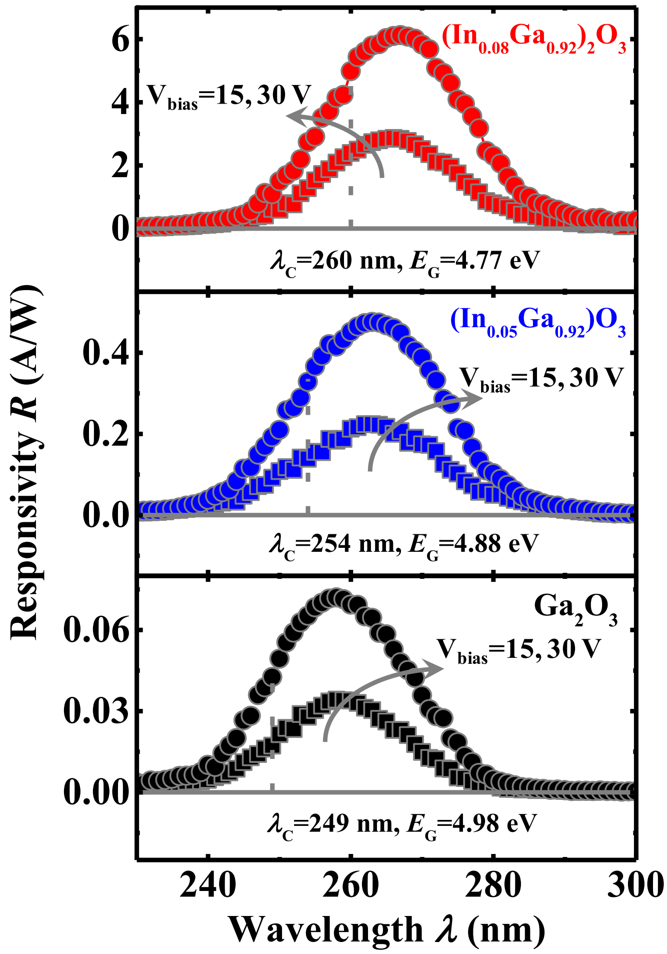

Fig. 8. R versus illumination wavelengths λ for the different photodetectors at $V_{bias} = 15$ and 30 V.

consist of two precedures, fast-response and slow-response. It is known that the defects levels in the bandgap might trap the photogenerated carriers and delay the carriers collection during UV light illumination or the recombination after switching off the light, leading to the slow-response, while the fast-response is associated with the band to band transition 0. The time constants τ_{r_1} and τ_{r_2} were determined to be 0.63(0.65@260 nm), 0.67, 0.82 sec and 6.59(6.68@260 nm), 5.19, 5.03 sec and those of decay process τ_{d_1} and τ_{d_2} were 0.52(0.57@260 nm), 0.48, 0.39 sec and 8.69(8.75@260 nm), 8.04, 5.73 sec for $(In_{0.08}Ga_{0.92})_2O_3$, $(In_{0.05}Ga_{0.95})_2O_3$ and Ga_2O_3 photodetectors, respectively. The larger time constant τ_{d2} of $(In_{0.08}Ga_{0.92})_2O_3$ suggests there are a greater number of defects in the bandgap, resulting in a larger persistent photoconductivity (PPC).

The R as a function of the illumination wavelengths λ for the fabricated devices is shown in the Fig. 8. A higher R was obtained in $(In_xGa_{1-x})_2O_3$ photodetectors, compared with Ga_2O_3 device. The maximum R (R_{max}) are 6.12A/W, 0.48A/W and 0.07A/W at the V_{bias} of 30 V for the three samples and the R_{max} shifts toward longer wavelengths with increasing In content. According to the equation $E_G = hc/\lambda_c$, where h is Planck's constant, c is velocity of light and λ_c is the cut-off wavelength corresponding to the direct bandgap 0, E_G of the fabricated photodetectors are calculated to be 4.77, 4.88 and 4.98 eV, respectively, illustrating the decrease of $(In_xGa_{1-x})_2O_3$ bandgap of for higher In composition, which is consistent with the transmittance and SE results.

4. Conclusion

We deposited single-crystal $(In_xGa_{1-x})_2O_3$ films on c-plane sapphire substrates using PLD. Compared with Ga_2O_3, the bandgap and conductivity is important for the $(In_xGa_{1-x})_2O_3$ film used for photodetectors. With the In composition increasing, the bandgap decrease and the cutoff wavelength will be red-shifted or shift to the lower energy. On the other hand, the larger the In composition, the higher the dark current and the enhanced I_{photo} and R, which is attributed to the incorporation of indium leading to the higher conductivity and lower Schottky barrier height. With the $(In_xGa_{1-x})_2O_3$ growth temperature decreasing, a higher In composition was obtained and a larger number of defects were also introduced into the $(In_xGa_{1-x})_2O_3$ films, resulting in the obvious PPC.

References

[1] M. Higashiwaki, K. Sasaki, A. Kuramata, T. Masui, and S. Yamakoshi, "Development of gallium oxide power devices," *Phys. Status Solidi (a)*, vol. 211, no. 1, pp. 21–26, 2014.

[2] K. Sasaki, M. Higashiwaki, A. Kuramata, T. Masui, and S. Yamakoshi, "MBE grown Ga_2O_3 and its power device applications," *J. Cryst. Growth*, vol. 378, pp. 591–595, 2013.

[3] W. Y. Kong *et al.*, "Graphene-β-Ga_2O_3 heterojunction for highly sensitive deep UV photodetector application," *Adv. Mater.*, vol. 28, no. 48, pp. 10725–10731, 2016.

[4] T. Oshima, T. Okuno, and S. Fujita, "Ga_2O_3 thin film growth on c-plane sapphire substrates by molecular beam epitaxy for deep-ultraviolet photodetectors," *Jpn. J. Appl. Phys.*, vol. 46, no.11, pp. 7217–7220, 2007.

[5] M. Zhong, Z. Wei, X. Meng, F. Wu, and J. Li, "High-performance single crystalline UV photodetectors of β-Ga_2O_3," *J. Alloys Compounds*, vol. 619, pp. 572–575, 2015.

[6] L. Huang *et al.*, "Comparison study of β-Ga_2O_3 photodetectors grown on sapphire at different oxygen pressures," *IEEE Photon. J.*, vol. 9, no. 4, Aug. 2017, Art. no. 6803708.

[7] Q. Feng, L. Huang, G. Han, F. Li, X. Li, and Y. Hao, "Comparison study of β-Ga_2O_3 photodetectors on bulk substrate and sapphire," *IEEE Trans. Electron Devices*, vol. 63, no. 9, pp. 3578–3583, Sep. 2016.

[8] Y. Kokubun, K. Miura, F. Endo, and S. Nakagomi, "Sol-gel prepared β-Ga_2O_3 thin films for ultraviolet photodetectors," *Appl. Phys. Lett.*, vol. 90, no. 3, p. 031912, 2007.

[9] F. Yang, J. Ma, C. Luan, and L. Kong, "Structural and optical properties of $Ga_{2(1-x)}In_{2x}O_3$ films prepared on α-Al_2O_3 (0001) by MOCVD," *Appl. Surf. Sci.*, vol. 255, no. 8, pp. 4401–4404, 2009.

[10] T. Oshima and S. Fujita, "Properties of Ga_2O_3-based $(In_xGa_{1--x})_2O_3$ alloy thin films grown by molecular beam epitaxy," *Phys. Status Solidi (c)*, vol. 5, no. 9, pp. 3113–3115, 2008.

[11] Y. Kokubun, T. Abe, and S. Nakagomi, "Sol–gel prepared $(Ga_{1-x}In_x)_2O_3$ thin films for solar-blind ultraviolet photodetectors," *Phys. Status Solidi (a)*, vol. 207, no. 7, pp. 1741–1745 2010.

[12] F. Zhang, K. Saito, T. Tanaka, M. Nishio, and Q. Guo, "Wide bandgap engineering of $(GaIn)_2O_3$ films," *Solid State Commun.*, vol. 186, pp. 28–31, 2014.

[13] T. Chang, S. Chang, C. J. Chiu, C. Wei, Y. Juan, and W. Weng, "Bandgap-engineered in indium–gallium–oxide ultraviolet phototransistors," *IEEE Photon. Technol. Lett.*, vol. 27, no. 8, pp. 915–918, Apr. 2015.

[14] M. Baldini, D. Gogova, K. Irmscher, M. Schmidbauer, G. Wagner, and R. Fornari, "Heteroepitaxy of $Ga_{2(1-x)}In_{2x}O_3$ layers by MOVPE with two different oxygen sources," *Cryst. Res. Technol.*, vol. 49, no. 8, pp. 552–557, 2014.

[15] Z. Zhang, H. Wenckstern, J. Lenzner, M. Lorenz, and M. Grundmann, "Visible-blind and solar-blind ultraviolet photodiodes based on $(In_xGa_{1-x})_2O_3$," *Appl. Phys. Lett.*, vol. 108, no. 12, p. 123503, 2016.

[16] D. Cho, "Chemical and structural properties of ternary post-transition metal oxide thin films: InZnO, InGaO and GaZnO," *Curr. Appl. Phys.*, vol. 15, no. 11, pp. 1337–1341, 2015.

[17] F. Zhang *et al.*, "Toward the understanding of annealing effects on $(GaIn)_2O_3$ films," *Thin Solid Films*, vol. 578, pp. 1–6, 2015.

[18] Z. Hu *et al.*, "Optical properties of $(Al_xGa_{1-x})_2O_3$ on sapphire," *Superlattices Microstruct.*, vol. 114, pp. 82–88, 2018.

[19] R. Schmidt-Grund, C. Kranert, T. Böntgen, H. von Wenckstern, H. Krauß, and M. Grundmann, "Dielectric function in the NIR-VUV spectral range of $(In_xGa_{1-x})_2O_3$ thin films," *J. Appl. Phys.*, vol. 116, no. 5, p. 053510, 2014.

[20] S. K. Gullapalli, R. S. Vemuri, and C. V. Ramana, "Structural transformation induced changes in the optical properties of nanocrystalline tungsten oxide thin films," *Appl. Phys. Lett.*, vol. 96, no. 17, p. 171903, 2010.

[21] T. Chang, S. Chang, W. Weng, C. Chiu, and C. Wei, "Amorphous indium–gallium–oxide UV photodetectors," *IEEE Photon. Technol. Lett.*, vol. 27, no. 19, pp. 2083–2086, Oct. 2015.

[22] H. von Wenckstern, D. Splith, A. Werner, S. Müller, M. Lorenz, and M. Grundmann, "Properties of Schottky barrier diodes on $(In_xGa_{1--x})_2O_3$ for $0.01 \leq x \leq 0.85$ determined by a combinatorial approach," *ACS Combinatorial Sci.*, vol. 17, no. 12, pp. 710–715 2015.

[23] H. von Wenckstern *et al.*, "Structural and optical properties of $(In,Ga)_2O_3$ thin films and characteristics of Schottky contacts thereon," *Semicond. Sci. Technol.*, vol. 30, no. 2, 2015, Art. no. 024005.